Addendum Cover Page

Complete only applicable items.

QA: QA

1. Total Pages: 44

2. Addendum to (Title):
Multiscale Thermohydrologic Model

3. DI (including Revision and Addendum No.):
ANL-EBS-MD-000049 REV03 AD 02

	Printed Name	Signature	Date
4. Originator	Thomas A. Buscheck	Thomas A. Buscheck	1/29/08
5. Independent Technical Reviewer	Sumit Mukhopadhyay	Sumit Mukhopadhyay	1/29/2008
6. Checker	Scott James	Scott James	1/29/08
8. QCS / QA Reviewer	Charles Beach	Charles P. Beach	1-29-08
7. Responsible Manager / Lead	Ernest Hardin	Ernest Hardin	1/29/08
8. Responsible Manager	M. Kathryn Knowles	M. Kathryn Knowles	1/29/08

9. Remarks

Change History	
10. Revision and Addendum No.	11. Description of Change
REV 03 AD 02	Initial Issue. Changes in response to DOE comments and for TBV resolution.

SUMMARY AND ORGANIZATION

The purpose of this addendum (Addendum 02) is to modify the parent report, in accordance with the governing procedure (SCI-PRO-006, *Models*) and *Technical Work Plan for: Additional Multiscale Thermal Hydrologic Modeling* (SNL 2006 [DIRS 178297]). As used in this addendum, the term "parent report" refers to Revision 03 of *Multiscale Thermohydrologic Model* (SNL 2007 [DIRS 181383]), including material presented in Addendum 01 of that report. Cross-references to sections, figures, tables, or appendices from Addendum 01 are distinguished by the designation "[a]", which provides a means for locating and differentiating like-numbered elements in the parent report (e.g., "Section 6.3" refers to a location in the report proper, while "Section 6.3[a]" refers to a location in Addendum 01).

In general, the modifications presented in this addendum address comments resulting from review of the parent report by the TSPA organization and by the U.S. Department of Energy (DOE). The specific modifications are as follows, each representing an issue identified in the parent report and addressed herein:

(1) Two figures and two tables are revised in Section 6.3.16 of the parent report.

(2) Section 6.3.20 is added to the end of Section 6.3 of the parent report.

(3) Text and figures are added to the ends of Sections 7.8 and 7.9 of the parent report.

(4) Section 8.5.9 is added after Section 8.5.8 of the parent report to address CR-5154.

(5) Additional references are added to Section 9 of the parent report.

(6) Text and figures are added to the end of Appendix X of the parent report.

The organization of this addendum corresponds to the major outline of the parent report and includes all sections mandated by the governing procedure (SCI-PRO-006), regardless of whether or not a mandated section is being modified. Mandated sections, in other words, are reproduced in this addendum for procedural compliance and convenience of cross-referencing, but may not contain actual modifications to the parent report. In such cases, the addendum section contains a bracketed statement of "No modification" under the section heading.

Conversely, sections not mandated by procedure (i.e., most subsections) are reproduced in this addendum only if they contain a modification to the corresponding section of the parent report, which is also true of any other addendum elements (i.e., figures, tables, equations, or appendices). Unless added as new elements not present in the parent report, the numbering of addendum elements such as figures, tables, equations, and appendices corresponds to the numbering in the parent report. Bracketed designators (e.g., "[b]") are added to all numbered elements in this addendum to distinguish them from corresponding elements in the parent report.

In every case, the modifications presented in this addendum are preceded by bracketed, italicized text explaining why the modification was made and how it relates to the corresponding element in the parent report. When appropriate, this explanatory text may cite page and paragraph numbers from the parent report for cross-referencing purposes.

INTENTIONALLY LEFT BLANK

CONTENTS

Page

INTENTIONALLY LEFT BLANK

FIGURES

Page

INTENTIONALLY LEFT BLANK

TABLES

Page

INTENTIONALLY LEFT BLANK

ACRONYMS AND ABBREVIATIONS

[Acronyms and abbreviations used in this addendum are listed and defined below. Certain acronyms are used but not defined in the addendum text itself in order to reflect the treatment of acronyms in the parent report.]

BWR	boiling water reactor (in reference to a waste package type)
CCDF	complementary cumulative distribution function
CSNF	commercial spent nuclear fuel
DDT	discrete heat source, drift-scale, thermal conduction (MSTHM submodel)
DHLW	defense high-level waste
DOE	U.S. Department of Energy
MSTHM	multiscale thermohydrologic model
PWR	pressurized water reactor (in reference to a waste package type)
RH	relative humidity
SAR	Safety Analysis Report
TH	thermal-hydrologic
TSPA	total system performance assessment
3-D	three-dimensional

INTENTIONALLY LEFT BLANK

1[b]. PURPOSE

[No modification to parent report.]

2[b]. QUALITY ASSURANCE

[No modification to parent report.]

3[b]. USE OF SOFTWARE

[No modification to parent report.]

4[b]. INPUTS

4.1[b] DIRECT INPUT

[The following corrections are to Table 4-1[a] of the parent report: (1) in the row for the model input labeled "End-to-end waste package spacing," the citation in the source column was changed from "SNL 2007 [DIRS 179466], Table 4-1" to "SNL 2007 [DIRS 179354], Table 4-4, Parameter 05-02"; (2) in the row for the model input labeled "Invert height from bottom of drift," the citation in the source column was changed from "SNL 2007 [DIRS 179466], Table 4-1" to "SNL 2007 [DIRS 179354], Figure 4-1," and the conversion of 1.321 m to (4'-4") was changed to (52"); (3) in the row for the model input labeled "Nominal weight of drip shield," the citation in the source column was changed from "SNL 2007 [DIRS 179466], Table 4-1" to "SNL 2007 [DIRS 179354], Table 4-2."]

Table 4-1[b]. Summary of Direct Input Data and Information Required by the MSTHM

Model Input	Value	Source
Design Information		
End-to-end waste package spacing	0.1 m	SNL 2007 [DIRS 179354], Table 4-4, Parameter 05-02
Invert height from bottom of drift	0.806 m	Source was the same as used for previous MSTHM calculations, but will be reconciled with the value of 1.321 m (52") from SNL 2007 [DIRS 179354], Figure 4-1 (see Section 6.3.19[a] for details)
Nominal weight of drip shield	5,000 kg	SNL 2007 [DIRS 179354], Table 4-2

4.2[b] CRITERIA

[No modification to parent report.]

4.3[b] CODES, STANDARDS, AND REGULATIONS

[No modification to parent report.]

5[b]. ASSUMPTIONS

[No modification to parent report.]

6[b]. SCIENTIFIC ANALYSIS DISCUSSION

6.2.12.1[b] Binning MSTHM Results for TSPA

[The following replaces the fourth and fifth sentences in the third paragraph on page 6-3[a] of the parent report, under Section 6.2.12.1[a]. Two references to "30th percentile" are changed to "10th percentile," as follows:]

The 10th percentile, glacial-transition climate, percolation flux at the base of the PTn geologic unit was used to determine the five subregions (see Figure VIII-1[a]). This approach is similar to the approach used in previous performance assessments (see Appendix VIII of the parent report), with a small difference being the use of the 10th percentile case rather than the "mean" case used in the parent report. The subregion assignments determined for the 10th percentile glacial-transition map were applied to all four percolation flux cases and to all four climate states.

6.3.16[b] Current MSTHM Results for the TSPA Base Case

[Two figures and two tables are slightly revised from those in the parent report. The small revisions result from the implementation of the weighting factors from the unit cell in Table 6.2-6[a] of the parent report. The unit cell has eight waste packages, two half waste packages and six full waste packages. The CCDF plots in Figures 6.3-77[a] and 6.3-77[a] of the parent report apply equal weights to the eight waste packages. The revised figures (Figures 6.3-77[b] and 6.3-78[b]) apply a weighting factor of 0.5 to the two half waste packages and a weighting factor of 1.0 to the six full waste packages. This change resulted in very minor changes to these figures. Note that these figures are included in the report for illustration purposes only. The other minor change to these figures involves the implementation of the weights in Table 6.3-48[a] of the parent report to produce the ensemble plot. The original ensemble plots were produced using equal weights for the seven host-rock thermal conductivity/percolation flux cases. Tables 6.3-49[a] and 6.3-50[a] of the parent report are revised to be consistent with the revisions to the figures discussed above.]

[The following replaces Figure 6.3-77[a] on page 6-39[a] of the parent report. The revised figure weights the respective waste package locations according to Table 6.2-6[a] of the parent report and implements the weights from Table 6.3-48[a] of the parent report for the ensemble.]

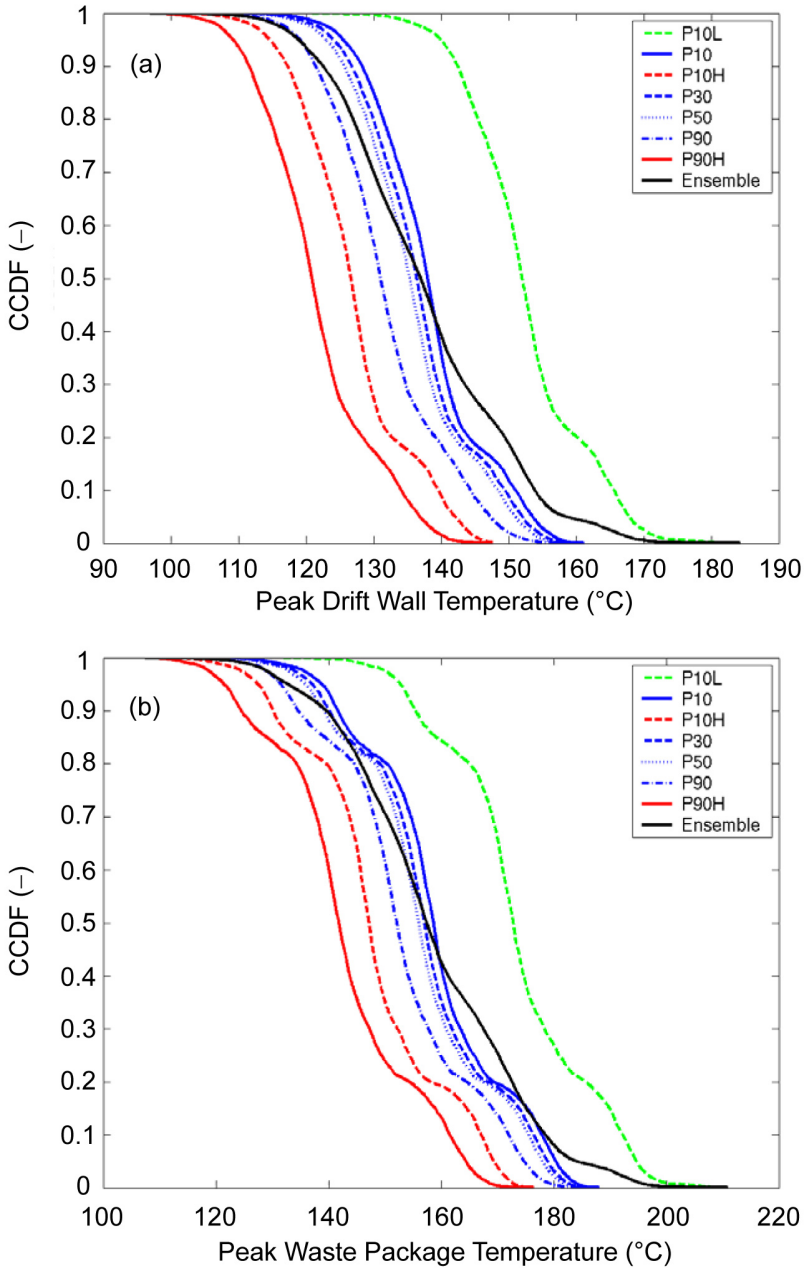

Source: Output DTNs: LL0702PA015MST.070, LL0702PA017MST.072, LL0702PA019MST.074, LL0702PA021MST.076, LL0702PA023MST.078, LL0702PA025MST.080, LL0702PA029MST.084, and MO0712THMHYDDP.000.

NOTE: Each of the seven CCDF plots represents 26,112 values, which is the product of eight different waste packages at 3,264 locations across the repository. These are the maximum temperatures corresponding to the 182,784 temperature histories in Figure 6.3-76[a] of the parent report. The ensemble is based on the data from the seven cases, using the weights from Table 6.3-48[a] of the parent report.

Figure 6.3-77[b]. CCDF for (a) Peak Drift Wall Temperature and (b) Peak Waste Package Temperature for the Range of Parametric Uncertainty Addressed by the MSTHM

[The following replaces Figure 6.3-78[a] on page 6-40[a] of the parent report. The revised figure weights the respective waste package locations according to Table 6.2-6[a] of the parent report and implements the weights from Table 6.3-48[a] of the parent report for the ensemble.]

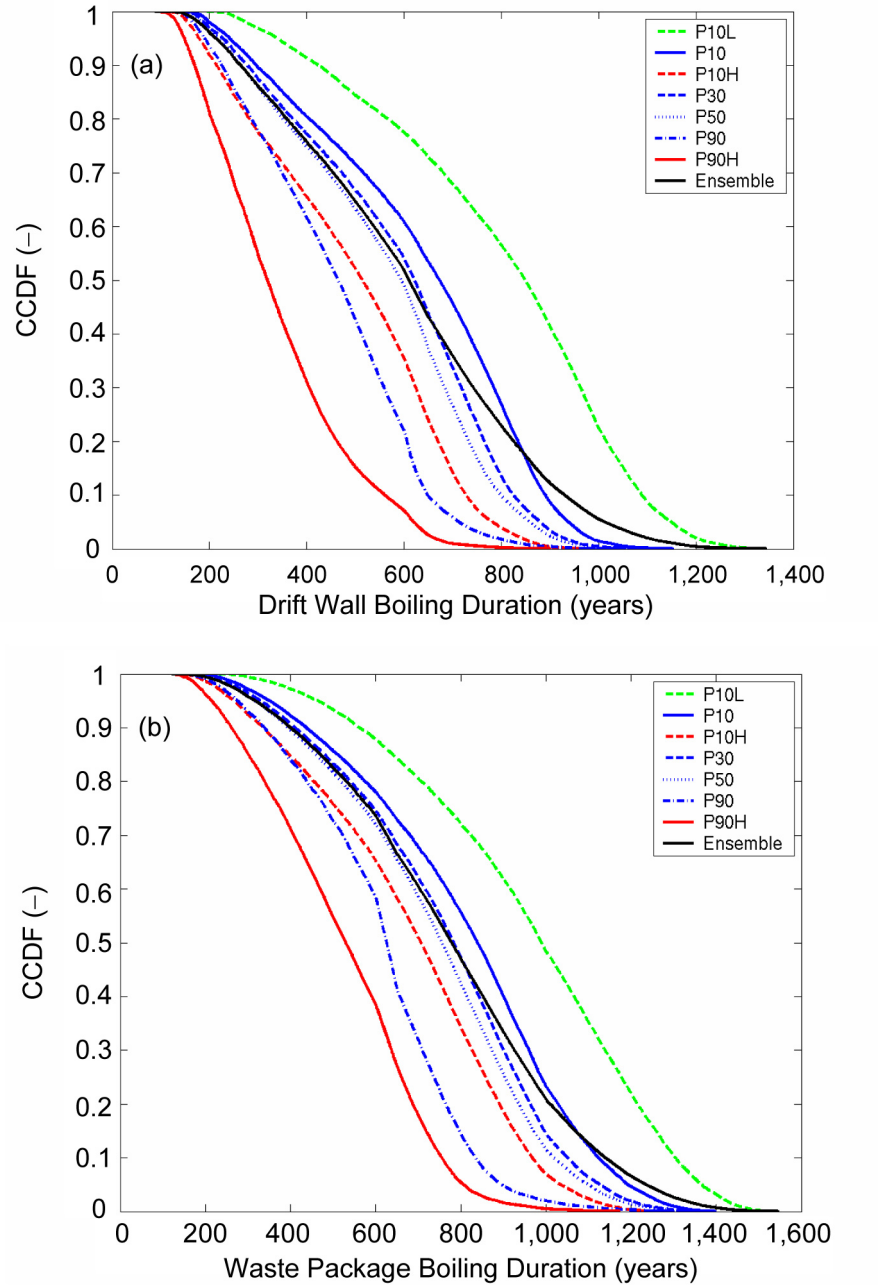

Source: Output DTNs: LL0702PA015MST.070, LL0702PA017MST.072, LL0702PA019MST.074, LL0702PA021MST.076, LL0702PA023MST.078, LL0702PA025MST.080, LL0702PA029MST.084, and MO0712THMHYDDP.000.

NOTE: Each of the seven CCDF plots represents 26,112 values, which is the product of eight different waste packages at 3,264 locations across the repository. These are the times when boiling ceases corresponding to the 182,784 temperature histories in Figure 6.3-76[a] of the parent report. The ensemble is based on the data from the seven cases, using the weights from Table 6.3-48[a] of the parent report.

Figure 6.3-78[b]. CCDF for the Time When Boiling Ceases on the (a) Drift Wall and (b) Waste Package for the Range of Parametric Uncertainty Addressed by the MSTHM

[The following replaces Tables 6.3-49[a] and 6.3-50[a] on page 6-41[a] of the parent report. The revisions to these tables are very minor, resulting from the minor revisions to Figures 6.3-77[a] and 6.3-78[a] of the parent report.]

Table 6.3-49[b]. Peak Drift Wall and Waste Package Temperatures Summarized for the Seven Modeled Uncertainty Cases

Infiltration Flux, Host-Rock Thermal Conductivity Case	Peak Drift Wall Temperature (°C)			Peak Waste Package Temperature (°C)		
	Coolest	Median	Hottest	Coolest	Median	Hottest
P10L (low K_{th})	120.5	152.0	184.3	131.6	172.8.	211.0
P10 (mean K_{th})	111.3	138.0	161.2	122.3	158.7	188.1
P10H (high K_{th})	102.7	126.6	149.5	113.5	147.2	176.5
P30 (mean K_{th})	109.2	136.4	160.5	120.1	157.0	187.3
P50 (mean K_{th})	107.8	135.3	159.6	118.8	156.0	186.4
P90 (mean K_{th})	103.8	131.0	159.6	114.6	152.1	186.4
P90H (high K_{th})	96.9	120.9	147.4	107.4	141.8	174.7
Ensemble[a]	96.9	137.0	184.3	107.4	157.4	211.0

Source: Output DTNs: LL0702PA015MST.070, LL0702PA017MST.072, LL0702PA019MST.074, LL0702PA021MST.076, LL0702PA023MST.078, LL0702PA025MST.080, LL0702PA029MST.084, and MO0712THMHYDDP.000.

[a] The ensemble is based on all of the data from the seven cases, weighted using the weights from Table 6.3-48[a] of the parent report.

NOTE: These cases cover the range of percolation flux and host-rock thermal conductivity uncertainty addressed in the parent report. This table is based on data plotted in Figure 6.3-77[b] of this addendum.

Table 6.3-50[b]. Time When Boiling Ceases at the Drift Wall Summarized for the Seven Modeled Uncertainty Cases

Infiltration Flux, Host-Rock Thermal Conductivity Case	Time When Boiling at the Drift Wall Ceases (years)						
	Shortest	10 Percentile	30 Percentile	Median	70 Percentile	90 Percentile	Longest
P10L (low K_{th})	189.2	423.9	680.2	848.9	962.9	1088.8	1345.1
P10 (mean K_{th})	148.5	295.7	516.6	672.6	784.7	890.0	1153.3
P10H (high K_{th})	115.2	214.4	363.8	514.5	624.1	727.5	968.9
P30 (mean K_{th})	139.0	277.2	471.8	621.5	718.0	824.5	1129.3
P50 (mean K_{th})	134.0	265.3	444.7	594.1	683.7	799.6	1114.4
P90 (mean K_{th})	116.3	224.9	348.9	464.3	559.0	648.3	1030.7
P90H (high K_{th})	87.3	169.3	243.6	319.1	405.0	560.6	900.8
Ensemble[a]	87.3	263.4	453.2	610.3	741.9	930.0	1345.1

Source: Output DTNs: LL0702PA015MST.070, LL0702PA017MST.072, LL0702PA019MST.074, LL0702PA021MST.076, LL0702PA023MST.078, LL0702PA025MST.080, LL0702PA029MST.084, and MO0712THMHYDDP.000.

[a] The ensemble is based on all of the data from the seven cases, weighted using the weights from Table 6.3-48[a] of the parent report.

NOTE: These cases cover the range of percolation flux and host-rock thermal conductivity uncertainty addressed in the parent report. This table is based on data plotted in Figure 6.3-78[b] of this addendum.

[The following section is added after Section 6.3.19[a] of the parent report to address relative humidity on waste packages during the post-thermal period.]

6.3.20[b] Relative Humidity on Waste Packages for the Post-Thermal Period

The purpose of this section is to investigate trends in the timing of predicted changes in relative humidity at the waste package surface, with an emphasis on the post-thermal period. For the purposes of this discussion the thermal period is defined to be the period when liquid-phase saturation in the host rock is drier than ambient conditions. After the emplacement drifts cool below the boiling point of water, moisture gradually returns to the near-field host rock, and *RH* eventually increases to nearly 100%. Resaturation of the host rock occurs more quickly for higher percolation flux than for lower percolation flux. Also, resaturation of the host rock occurs more quickly for higher host-rock thermal conductivity (because of cooler temperatures) than it does for lower host-rock thermal conductivity. Accordingly, elevated temperature conditions persist longer for lower percolation flux than for higher percolation flux and for lower host-rock thermal conductivity than for higher host-rock thermal conductivity. Thus, the duration of the thermal period varies as a function of host-rock thermal conductivity and percolation flux. The duration of the thermal period also depends on the proximity to the repository edge and heat output for a particular waste package.

A useful indicator of the duration of the thermal period is the time when boiling ceases at the drift wall. As shown in Table 6.3-50[b] of this addendum, the time when boiling ceases on the drift wall ranges from 87.3 to 1345.1 years, with the shortest time corresponding to a DHLW waste package at the repository edge in the P90H case, and the longest time corresponding to a PWR CSNF waste package at a "hot" location at the repository center for the P10L case. Table 6.2-6[a] of the parent report shows that the pwr1-3 waste package is the "hottest" waste package location in the MSTHM "unit cell."

Figures 6.3-98[b] and 6.3-99[b] plot complementary cumulative distribution functions (CCDFs) for the time required for relative humidity at the waste package surface to achieve 95% and 98%, respectively, for the seven percolation flux/host-rock thermal conductivity cases (P10L, P10, P10H, P30, P50, P90, and P90H; see Table 6.3-47[a] of the parent report). In these *RH* results, waste packages fall into three distinct groups: DHLW, BWR CSNF, and PWR CSNF waste packages, as noted on the figures. Table 6.2-6[a] of the parent report shows that the eight waste packages simulated in the MSTHM "unit cell" arrangement fall into these same three groups with respect to the rates of heat generation. Heat generation rates for the DHLW waste packages are smallest, allowing DHLW waste package *RH* to increase to 95% early during cooldown. The hottest and driest percolation flux/thermal conductivity case (P10L) takes the longest time to do this, while the coolest and wettest case (P90H) takes the shortest time. From left to right in the upper left corner of Figure 6.3-98[b], the seven cases are ordered as follows: P90H, P90, P50, P30, P10H, P10, and P10L. The reason for this trend is that hotter cases (e.g., P10L) result in greater (and more persistent) host-rock dryout and, hence, lower *RH* (and more persistent *RH* reduction) in the host rock at the drift wall than cooler cases (e.g., P90H).

The influence of the edge-cooling effect on DHLW waste packages is also evident, with waste packages closer to the repository edge cooling earlier, represented by the earliest part of the indicated step in the CCDF curve (Figure 6.3-98[b]). Waste packages closer to the repository

center take longer to cool, and are represented by the later part of the step. DHLW waste packages are the only waste packages that attain an *RH* of 95% during the boiling period, while the drift wall temperature exceeds the boiling point of water (maximum of 1,345 years; see Table 6.3-50[b] of this addendum), as indicated in Figure 6.3-98[b]. No waste packages attain an *RH* of 98% during this period (Figure 6.3-99[b]).

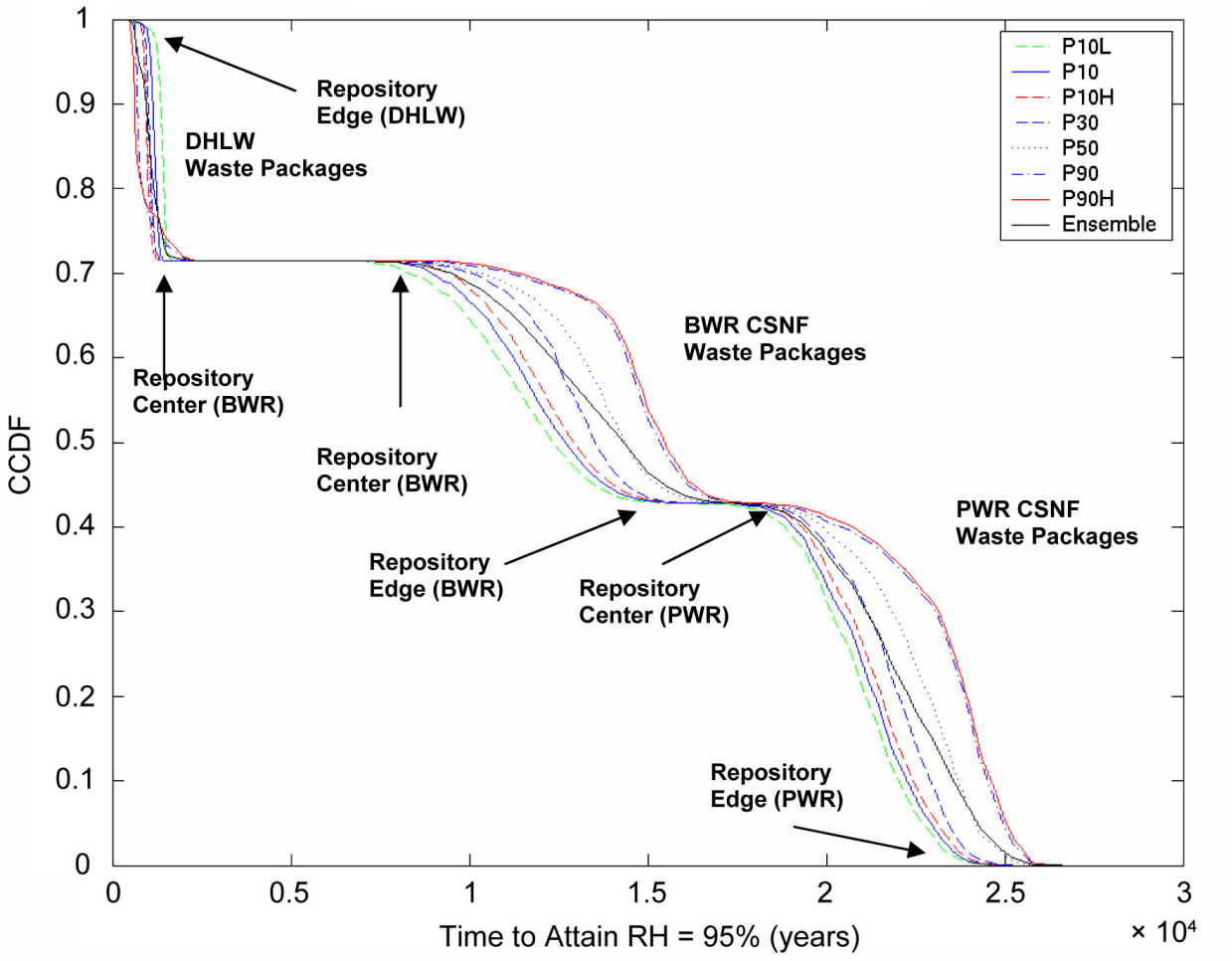

Output DTN: MO0712THMHYDDP.000.

NOTE: Each of the seven CCDF plots represents 26,112 values, which is the product of eight different waste packages simulated by the MSTHM, at 3,264 locations across the repository. These are the times when *RH* at the waste package surface increases to 95%, corresponding to the 182,784 *RH* histories in Figure 6.3-81b[a]. The ensemble is based on all of the data from the seven cases, weighted using the weights from Table 6.3-48[a]. The waste packages fall into three distinct groups: DHLW, BWR CSNF, and PWR CSNF waste packages.

Figure 6.3-98[b]. CCDF for the Time Required for Waste Package Relative Humidity to Attain a Value of 95%

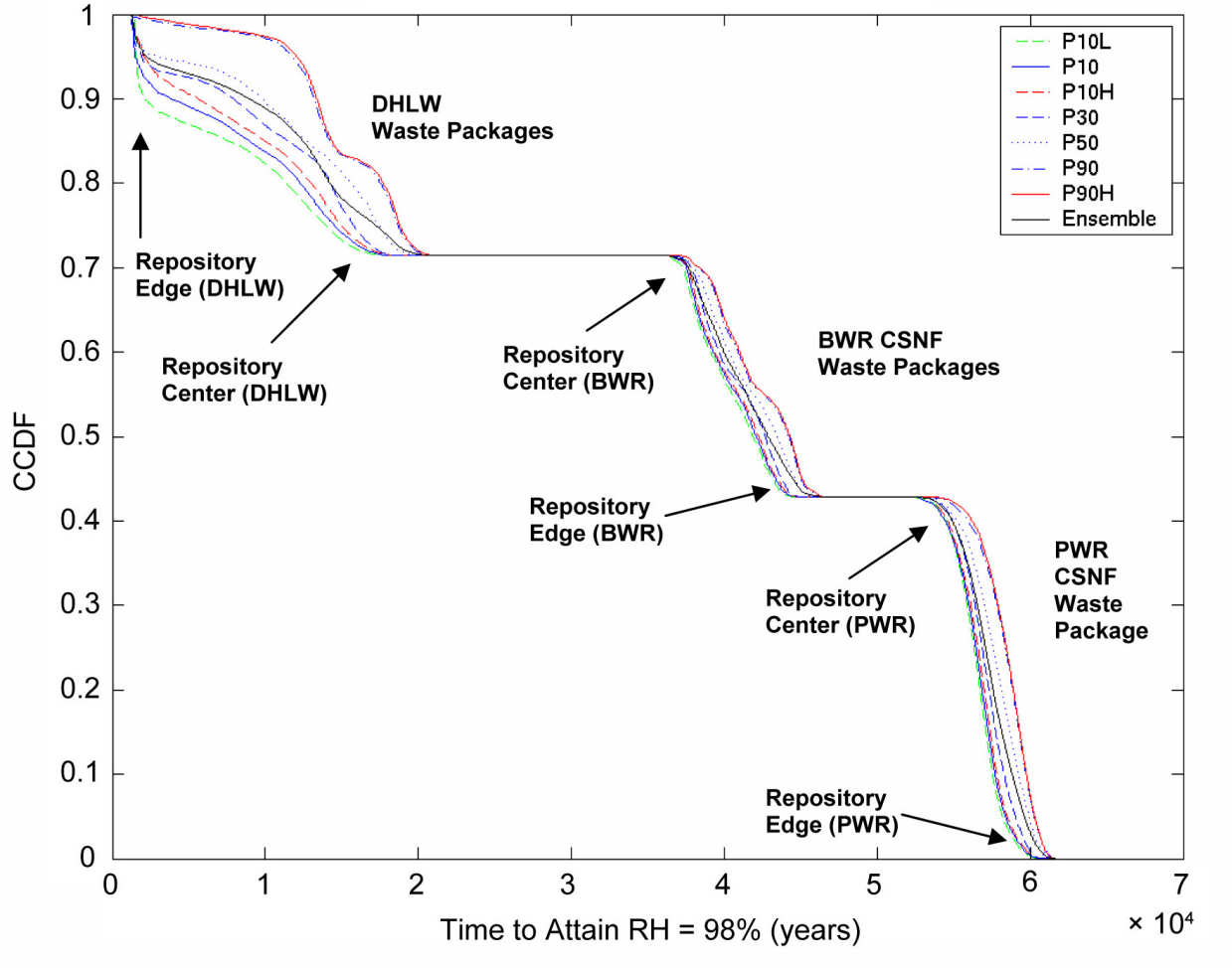

Output DTN: MO0712THMHYDDP.000.

NOTE: Each of the seven CCDF plots represents 26,112 values, which is the product of eight different waste packages simulated by the MSTHM, at 3,264 locations across the repository. These are the times when *RH* at the waste package surface increases to 98%, corresponding to the 182,784 *RH* histories in Figure 6.3-81b[a]. The ensemble is based on all of the data from the seven cases, weighted using the weights from Table 6.3-48[a]. The waste packages fall into three distinct groups: DHLW, BWR CSNF, and PWR CSNF waste packages.

Figure 6.3-99[b]. CCDF for the Time Required for Waste Package Relative Humidity to Attain a Value of 98%

For the post-thermal period, after the boiling period discussed above, the trend in *RH* for CSNF waste packages is the reverse of what it is for DHLW waste packages during the boiling period. As indicated in Figures 6.3-98[b] and 6.3-99[b], hotter cases (e.g., P10L) take less time to attain *RH* of 95% or 98% than cooler cases (e.g., P90H).

The "reversed" trend discussed above in *RH* for CSNF waste packages during the post-boiling period has a simple physical explanation. As discussed earlier, after the emplacement drifts cool below the boiling point of water, moisture gradually returns to the near-field host rock, and humidity increases. Where the background percolation flux is greater, relative humidity increases more quickly because water is more readily available to resaturate the rock. With greater liquid-phase saturation, the rock has greater thermal conductivity, and tends to cool

faster. In addition, percolation flux tends to remove sensible heat by warming of the downward convecting water. Hence, the host rock, represented by the drift wall temperature, cools faster with greater percolation flux.

Heat transfer within the drift is predominantly radiative, compared with thermal conduction that dominates in the host rock. Heat transfer from a waste package to the drip shield and then to the drift wall causes temperature differences that depend on the power transferred, the thermal emissivities of the materials, and the geometry of the radiating surfaces. Importantly, the temperature differences are nearly independent of the actual temperatures over the temperature range of interest. In other words, the temperature difference between the waste package and the drift wall is rather insensitive to the average temperature of the system. Radiative heat transfer follows the Stefan-Boltzmann law (Incropera and DeWitt 1996 [DIRS 108184], p. 9) and is proportional to the difference of the absolute temperatures to the fourth power. A slightly greater temperature difference is needed to transmit the same power at lower temperature, but the effect is not important to this analysis.

The drift wall gradually cools by conduction of heat (radially and vertically) outward toward a fixed far-field temperature. The waste package and drip shield temperatures are controlled by the predominantly radiative temperature differences described above, which are added to the drift wall temperature. If the drift wall cools more quickly because of greater percolation flux, or greater host-rock thermal conductivity, the same radiative temperature differences are added to a cooler drift wall temperature. Moreover, these radiative temperature differences are larger at earlier time, because waste package thermal output decays steadily with time. This means that radiative temperature differences between the waste package and drift wall increase weakly with percolation flux and with thermal conductivity in the host rock.

Absolute humidity in the drift (i.e., the fraction of moisture in the air) is controlled by *RH* at the drift wall, which is controlled by hydrologic processes in the host rock. Relative humidity (*RH*) is the ratio of the partial pressure of water vapor P_v, to the temperature-dependent saturated vapor pressure $P_{sat}(T)$ at the local temperature T:

$$RH_{dw} = \frac{P_v}{P_{sat}(T_{dw})} \qquad RH_{WP} = \frac{P_v}{P_{sat}(T_{WP})} \qquad \text{(Eq. 6.3-1[b])}$$

where the subscripts *dw* and *WP* signify the drift wall and waste package, respectively, and P_v is the partial pressure of water vapor in the well-mixed air of the drift. For the post-thermal period, the explanation presented here assumes that *RH* at the drift wall is very close to 100%, which occurs well within 2,000 years, after the host rock has rewet to ambient conditions. The temperature difference between the waste package and the drift wall then determines *RH* at the waste package:

$$RH_{WP} = \frac{P_v}{P_{sat}(T_{WP})} \approx \frac{P_{sat}(T_{dw})}{P_{sat}(T_{WP})} = \frac{RH_{WP}}{RH_{dw}} \qquad \text{(Eq. 6.3-2[b])}$$

The behavior of $P_{sat}(T_{dw})/P_{sat}(T_{WP})$ as a function of T_{dw} is shown in Figure 6.3-100[b]. For a given temperature difference ($\Delta T = T_{WP} - T_{dw}$) and RH_{dw}, RH_{WP} decreases with decreasing T_{dw}. Whether caused by higher percolation flux, higher host-rock thermal conductivity, or closer

proximity to the repository edge, cooler waste packages are drier than warmer waste packages for a given waste package heat output.

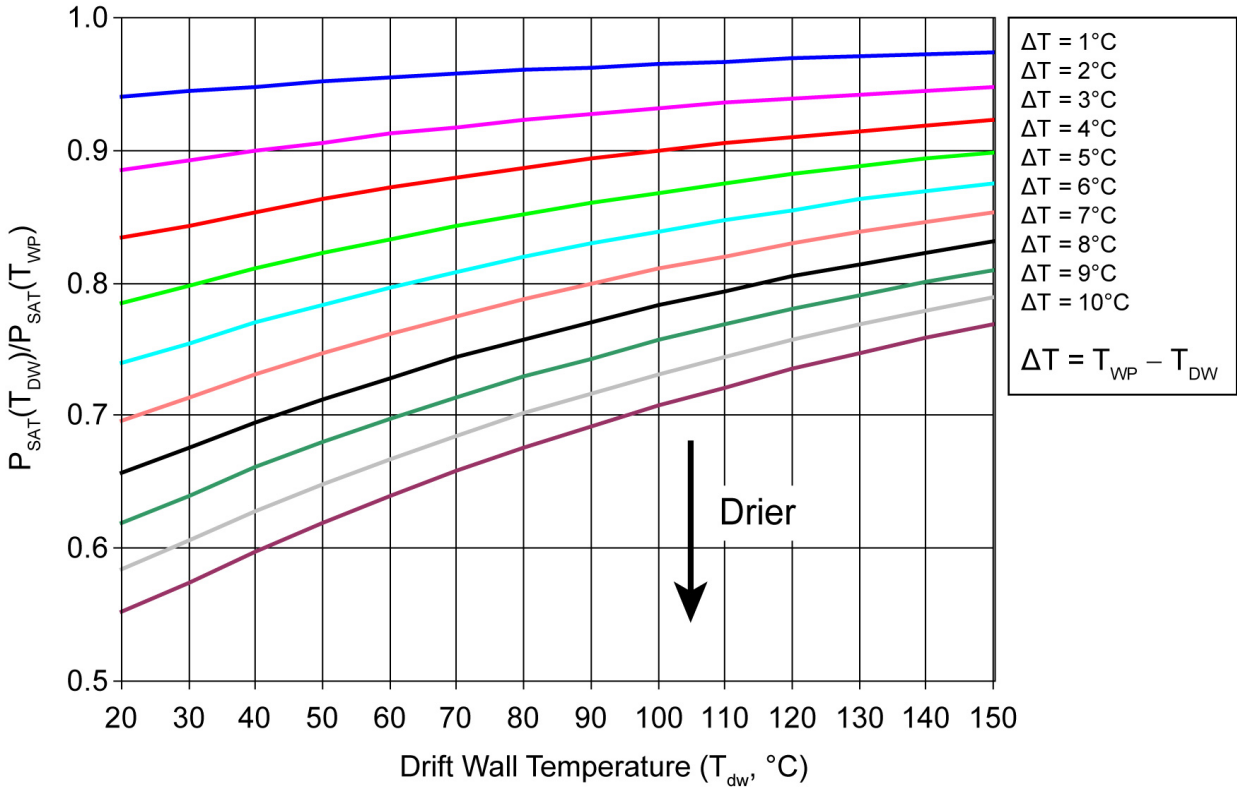

Output DTN: MO0712THMHYDDP.000.

NOTE: The saturated vapor pressure is obtained from the steam tables (Keenan et al. 1969 [DIRS 134666]). The saturated vapor pressure ratio is determined for different values of temperature difference between the waste package and drift wall.

Figure 6.3-100[b]. Saturated Vapor Pressure Ratio as a Function of Drift Wall Temperature

Finally, the foregoing discussion did not mention variability in heat output for adjacent or nearby waste packages. Higher heat-output waste packages are drier than lower heat-output waste packages for a given drift wall temperature. The range of variability in waste package temperature and *RH* at any particular time will increase with the range of waste package heat output. As long as thermal radiation remains the dominant mode of heat transfer within the drifts, the temperature differences between each waste package and the drift wall will be insensitive to the average temperature of the system, and cooler waste packages will be drier than warmer waste packages for a given waste package heat output. The second-order effect of ΔT increasing weakly with decreasing T_{dw} also contributes to cooler waste packages being drier than warmer waste packages for a given waste package heat output.

If the *RH* at the drift wall is less than 100%, i.e., $P < P_{sat}(T_{dw})$, the argument still applies because the effects on *RH* at the drip shield and waste package cancel. Letting $RH_{dw} = P_v / P_{sat}(T_{dw})$, with RH_{dw} less than but close to 100%, gives:

$$RH_{WP} = \frac{RH_{dw} P_{sat}(T_{dw})}{P_{sat}(T_{WP})} \approx \frac{P_{sat}(T_{dw})}{P_{sat}(T_{WP})} = \frac{RH_{WP}}{RH_{dw}} \qquad \text{(Eq. 6.3-3[b])}$$

so that the behavior represented by Figure 6.3-100[b] still applies. Hence, the possibility of lower absolute humidity in the drift does not change the tendency for cooler overall conditions (as are caused by greater percolation flux, higher host-rock thermal conductivity, or greater proximity to the repository edge) to produce lower *RH* on waste packages with a given heat output compared with hotter conditions (caused by smaller percolation flux, lower host-rock thermal conductivity, or less proximity to the repository edge).

It is worth noting that the lower heat output associated with DHLW waste packages results in a very small temperature difference between the waste package and drift wall. This is particularly true at later times, as a result of the decaying time-dependent heat output. Consequently, once *RH* at the drift wall has approached 95%, Equation 6.3-3[b] has also approached 95% for all DHLW waste packages. Thus, *RH* reduction on DHLW waste packages is always dominated by *RH* reduction at the drift wall, and the reversed *RH* trend discussed above for the CSNF waste packages does not apply to DHLW waste packages.

Recall the observation that Figures 6.3-98[b] and 6.3-99[b] show three distinct groups of waste packages. The sloping portion of CCDF curves in the upper left of those figures represents the DHLW waste packages; the sloping portion of the CCDF curves in the center represents BWR CSNF waste packages, and the sloping portion of the CCDF curves in the lower right represents PWR CSNF waste packages. The "plateau" portions of the CCDF curves show how distinctive the three groups of waste packages are with respect to late time *RH* histories. For CSNF waste packages, the CCDF curve furthest to the right of the sloping portions of the CCDF curves corresponds to the coolest case (P90H), while the CCDF curve furthest to the left corresponds to the hottest case (P10L). From left to right, the seven cases are ordered as follows: P10L, P10, P10H, P30, P50, P90, and P90H. The edge-cooling effect causes the actual slope of those portions of the respective CCDF curves. CSNF waste package locations closer to the repository center are hotter (and more humid) than waste package locations closer to the edges. Consequently, waste packages closer to the repository center are represented by the upper left of the sloping portions of the CCDF curves for CSNF waste packages, while waste packages closer to the repository edges are represented by the lower right of the sloping portions of the CCDF curves (Figures 6.3-98[b] and 6.3-99[b]).

7[b]. VALIDATION

7.8[b] COMPARISON OF THE MSTHM RESULTS AGAINST A THREE-DIMENSIONAL PILLAR-SCALE THERMAL-HYDROLOGICAL MODEL

[The following text is added to the end of Section 7.8[a] of the parent report, to expand the validation discussion for the MSTHM predictions of invert liquid-phase saturation and temperature.]

The following information on invert temperature and liquid-phase saturation as represented by the MSTHM, compared to predictions from the 3-D pillar-scale validation cases, provides additional confidence that the MSTHM invert results are adequate for the intended use in TSPA. This information supplements discussion of invert properties and depth provided in the parent report (Sections 6.3.3 and 6.3.11; Sections 6.2.13.2[a] and 6.3.19[a]). A summary of this additional information combined with that provided in the parent report is provided in Section 7.9[b].

Validation comparisons between the MSTHM results and those of a 3-D pillar-scale TH model (Figures 7.8-2[a] through 7.8-9[a] in the parent report) are extended to include comparison of predicted average temperature within the invert (Figures 7.8-10[b] through 7.8-17[b]). The comparison includes two cases from the 3-D pillar-scale TH model (see Section 7.8[a] of the parent report). Case 1 allows advective and diffusive vapor transport in the longitudinal direction along the drift, while Case 2 does not allow such transport in the longitudinal direction, but does allow radial advective and diffusive vapor transport in the drift.

Figures 7.8-2[a] through 7.8-9[a] in the parent report show the *intragranular* liquid-phase saturation in the invert ballast material, which approaches zero during the peak thermal period, then recovers, approaching 100% during cooldown, after the boiling period. The intergranular liquid-phase saturation remains small during and after the boiling period, which is reasonable because the invert (like the host rock) is free-draining for all conditions likely to occur. The invert ballast has ample excess intergranular permeability to drain any liquid flux that may occur, so long as intergranular liquid-phase saturation does not exceed a few percent.

Reasonable agreement is obtained for predicted invert liquid-phase saturation, as discussed in Section 7.5.4 of the parent report. Additional sensitivity studies presented in Sections 6.3.3, 6.3.11, and 6.3.14[a] of the parent report show that output from the MSTHM is insensitive to uncertainty in invert hydrologic properties. The invert rewets by condensation and wicking from the host rock, so that the invert liquid-phase saturation tracks changes in the host-rock *RH*. This is reasonable because the invert has a small capacity for unsaturated water storage compared to that of the surrounding host rock, so that invert liquid-phase saturation changes cannot significantly affect the local *RH*. Hence, the invert liquid-phase saturation behavior predicted by the MSTHM is physically reasonable and consistent with other predictions used in TSPA, and is adequate for use in TSPA to represent diffusive transport of radionuclides (SNL 2007 [DIRS 177407], Section 6.5.2.3) and invert chemical conditions that affect radionuclide solubility and colloid stability (SNL 2007 [177412], Section 6.15.2; see Appendix XV of the parent report).

Uncertainty in the invert hydrologic properties translates to uncertainty in the volumetric moisture content, for a given *RH* in the drift environment, that could affect how radionuclide transport is represented in TSPA. However, uncertainty in the volumetric moisture content of the invert ballast is accommodated in the treatment of radionuclide transport properties (SNL 2007 [DIRS 177407], Section 6.3.4.1.1). The approach also justifies representing the invert hydrologic properties by a "point solution," i.e., using the single set of values developed in Appendix X[a] of the parent report.

Reasonable agreement is also obtained for predicted invert temperature between the 3-D pillar-scale TH model and the MSTHM results (Figures 7.8-10[b] through 7.8-17[b]). The behavior of invert temperature is essentially the same as the agreement in predicted drift wall and waste package temperatures (Section 7.8[a]) and as shown in Figures 7.8-2[a] through 7.8-9[a] of the parent report. For all eight waste packages simulated in the MSTHM, closest agreement for both invert temperature and liquid-phase saturation, between the MSTHM and 3-D pillar-scale TH model, is obtained at the repository center, which represents the overwhelming majority of waste packages in the repository.

For waste packages located near the repository edge, inspection of Figures 7.8-10[b] through 7.8-17[b] shows that for the seventh waste package from the edge, all the way to the repository center, the MSTHM and 3-D pillar-scale TH model are in close agreement. For the outermost six waste packages, the MSTHM predicts higher invert temperatures for early time (including when temperatures peak), and the agreement improves gradually with time. These results are consistent with previously discussed trends in waste package temperature and *RH* (Sections 7.5.2.4 and 7.5.2.5 of the parent report), which were found to affect only a small percentage of the overall number of waste package locations in the repository.

As discussed in Section 7.8[a] of the parent report, the cause of this overprediction of temperature at the repository edge is the dimensionality of the DDT submodel. The use of an additional, more complex DDT submodel with an unheated portion in the axial direction (i.e., beyond the outermost waste package) would capture the influence of axial heat flow (primarily by thermal radiation) for the outermost waste packages. The implementation of such a DDT submodel in the MSTHM would result in closer agreement in temperatures between the MSTHM and the 3-D pillar-scale TH model.

The invert temperature and liquid-phase saturation responses exhibit the same trends, and the largest differences between the MSTHM and the 3-D pillar-scale TH model decrease with time, becoming insignificant after cooldown. The magnitude of the differences for invert liquid-phase saturation was found to be small compared to the range of variation attributed to uncertainty in percolation flux and host-rock thermal conductivity (Section 7.5.4 of the parent report), and, by analogy, the same conclusion may be inferred for invert temperature. Hence, the invert temperature predicted by the MSTHM is physically reasonable and consistent with other predictions used in TSPA, and is adequate for use in TSPA to represent diffusive transport of radionuclides (SNL 2007 [DIRS 177407], Section 6.5.2.3) and invert chemical conditions that affect radionuclide solubility and colloid stability (SNL 2007 [177412], Section 6.15.2; see Appendix XV of the parent report).

Invert temperature depends on thermal conductivity for the invert ballast, a parameter developed in Section X.3[a] of the parent report. Additional confidence building information is provided in Section X.1[a], drawing on sensitivity analyses in Sections 6.3.2 and 6.3.19[a] of the parent report, and showing that the value used in the MSTHM is reasonable, and that the MSTHM results for other measures such as drift wall temperature and *RH* are relatively insensitive to heat transfer in the invert.

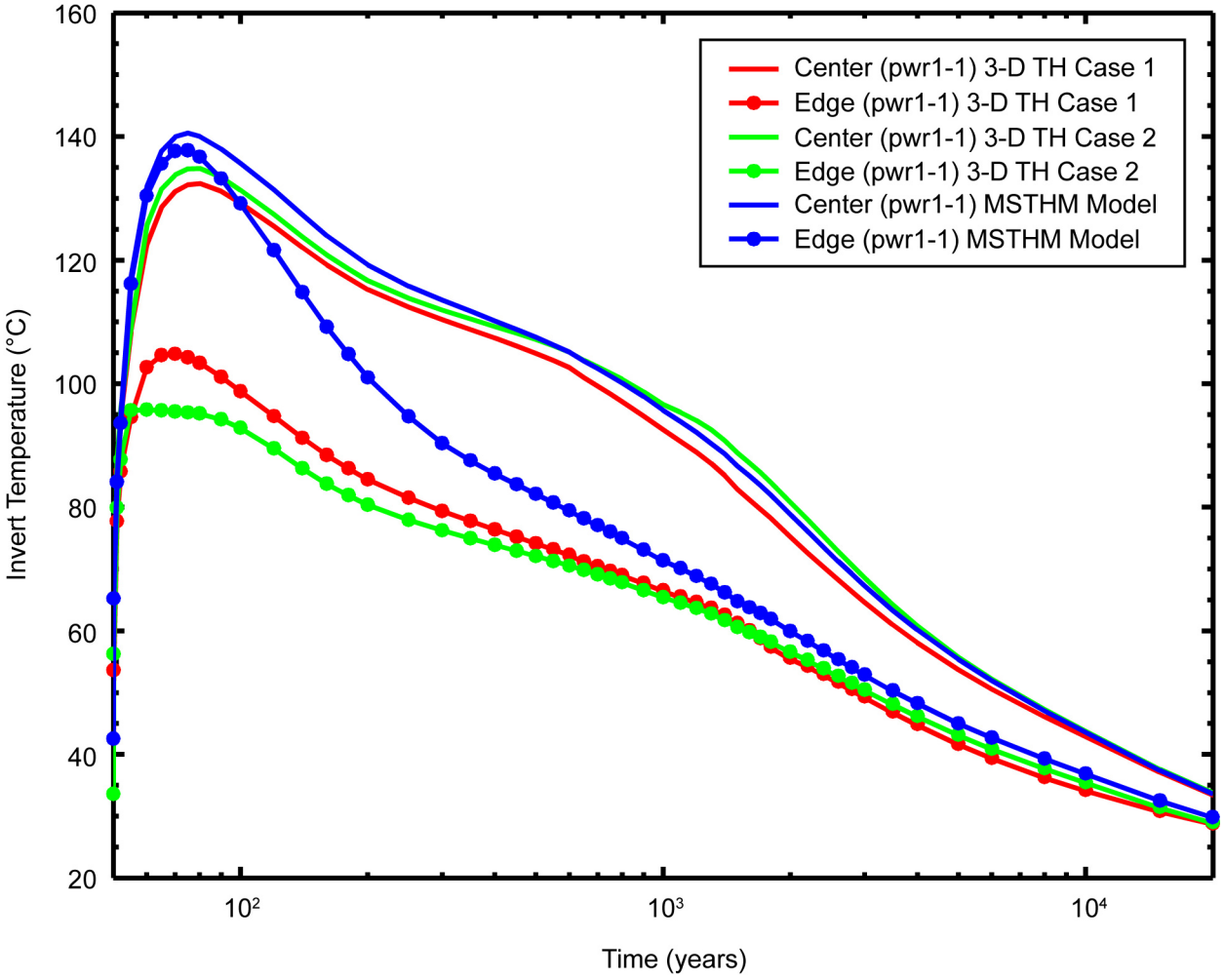

Source: Output DTN: LL0705PA032MST.028.

NOTE: For the 3-D pillar-scale TH model, Case 1 allows advective and diffusive vapor transport along a drift, while Case 2 does not. These results are for the pwr1-1 waste packages located at the repository center and edge. At the repository edge, the pwr1-1 is the outermost waste package.

Figure 7.8-10[b]. Invert Temperature Predicted by the MSTHM and 3-D Pillar-Scale TH Model Compared at the Repository Center and Edge for the pwr1-1 Waste Package

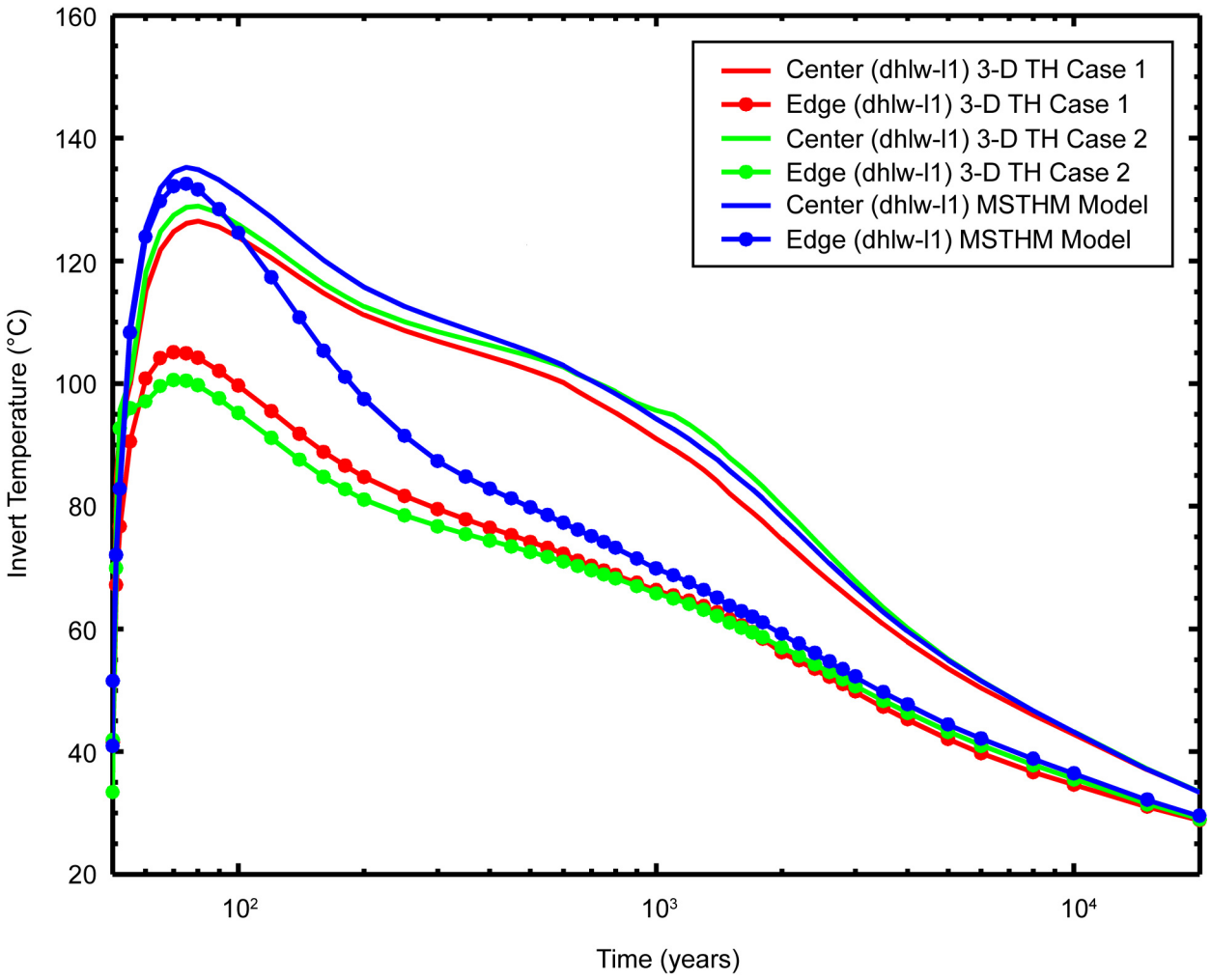

Source: Output DTN: LL0705PA032MST.028.

NOTE: For the 3-D pillar-scale TH model, Case 1 allows advective and diffusive vapor transport along a drift, while Case 2 does not. These results are for the dhlw-l1 waste packages located at the repository center and edge. At the repository edge, the dhlw-l1 is the second waste package from the edge.

Figure 7.8-11[b]. Invert Temperature Predicted by the MSTHM and 3-D Pillar-Scale TH Model Compared at the Repository Center and Edge for the dhlw-l1 Waste Package

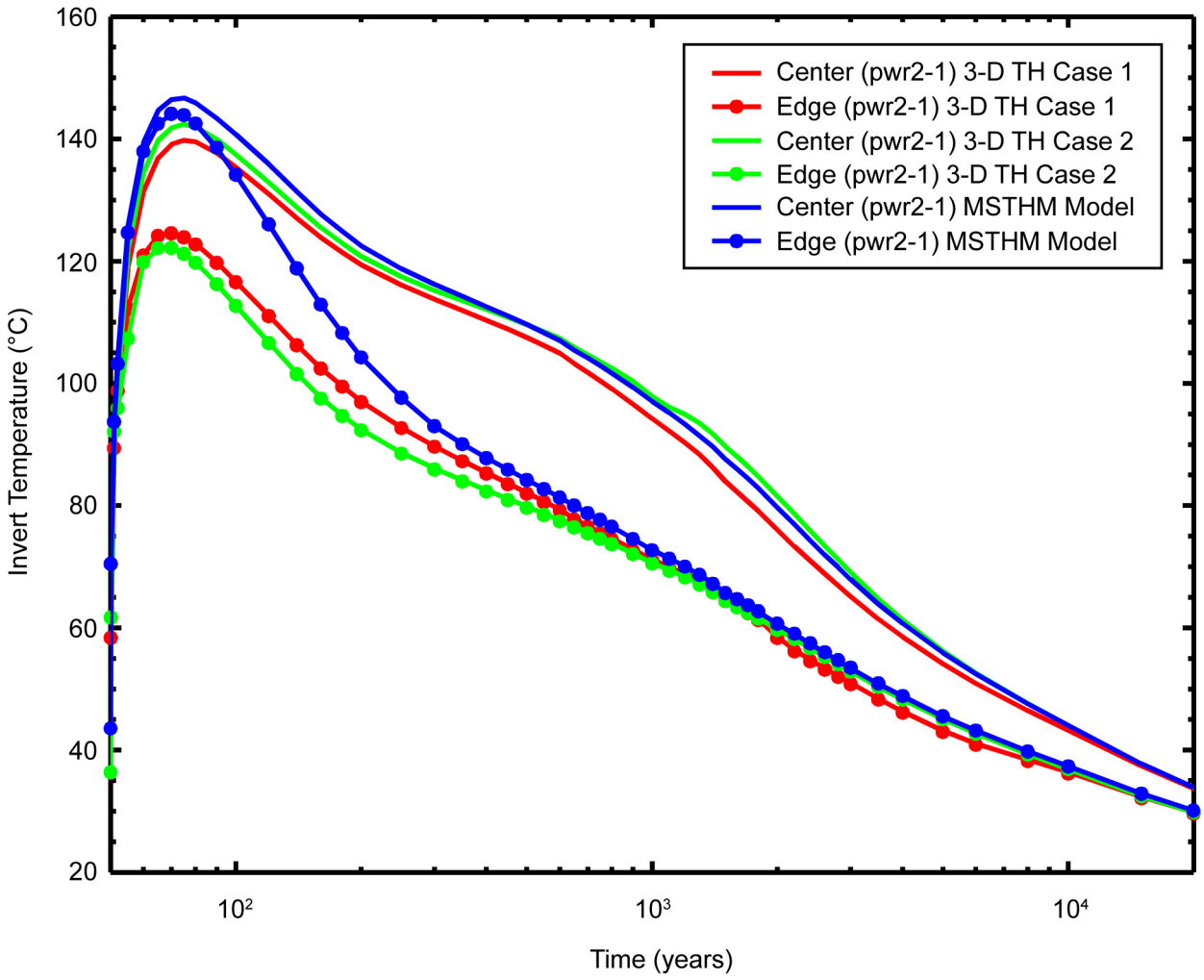

Source: Output DTN: LL0705PA032MST.028.

NOTE: For the 3-D pillar-scale TH model, Case 1 allows advective and diffusive vapor transport along a drift, while Case 2 does not. These results are for the pwr2-1 waste packages located at the repository center and edge. At the repository edge, the pwr2-1 is the third waste package from the edge.

Figure 7.8-12[b]. Invert Temperature Predicted by the MSTHM and 3-D Pillar-Scale TH Model Compared at the Repository Center and Edge for the pwr2-1 Waste Package

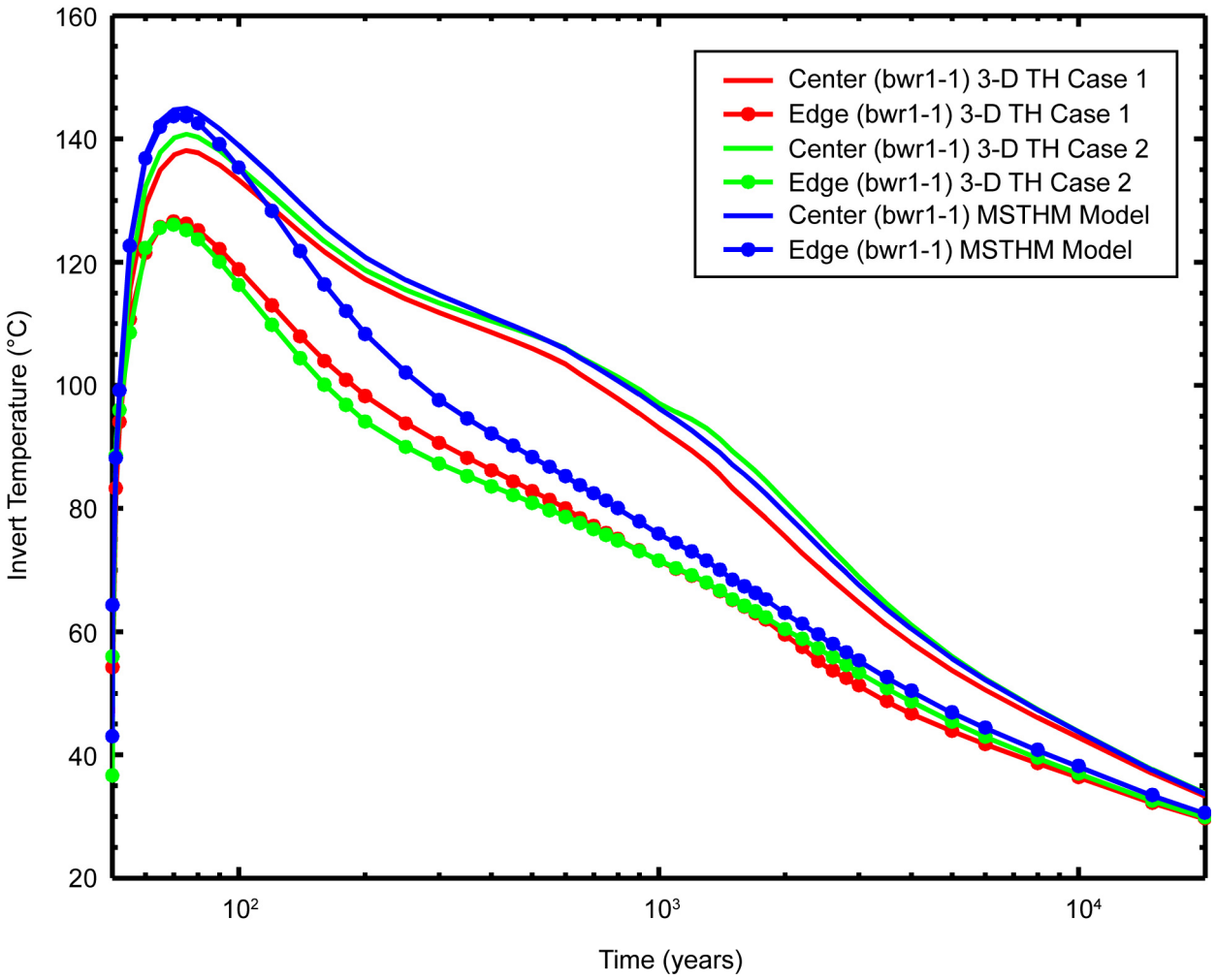

Source: Output DTN: LL0705PA032MST.028.

NOTE: For the 3-D pillar-scale TH model, Case 1 allows advective and diffusive vapor transport along a drift, while Case 2 does not. These results are for the bwr1-1 waste packages located at the repository center and edge. At the repository edge, the bwr1-1 is the fourth waste package from the edge.

Figure 7.8-13[b]. Thermal-Hydrologic Conditions Predicted by the MSTHM and 3-D Pillar-Scale TH Model Compared at the Repository Center and Edge for the bwr1-1 Waste Package

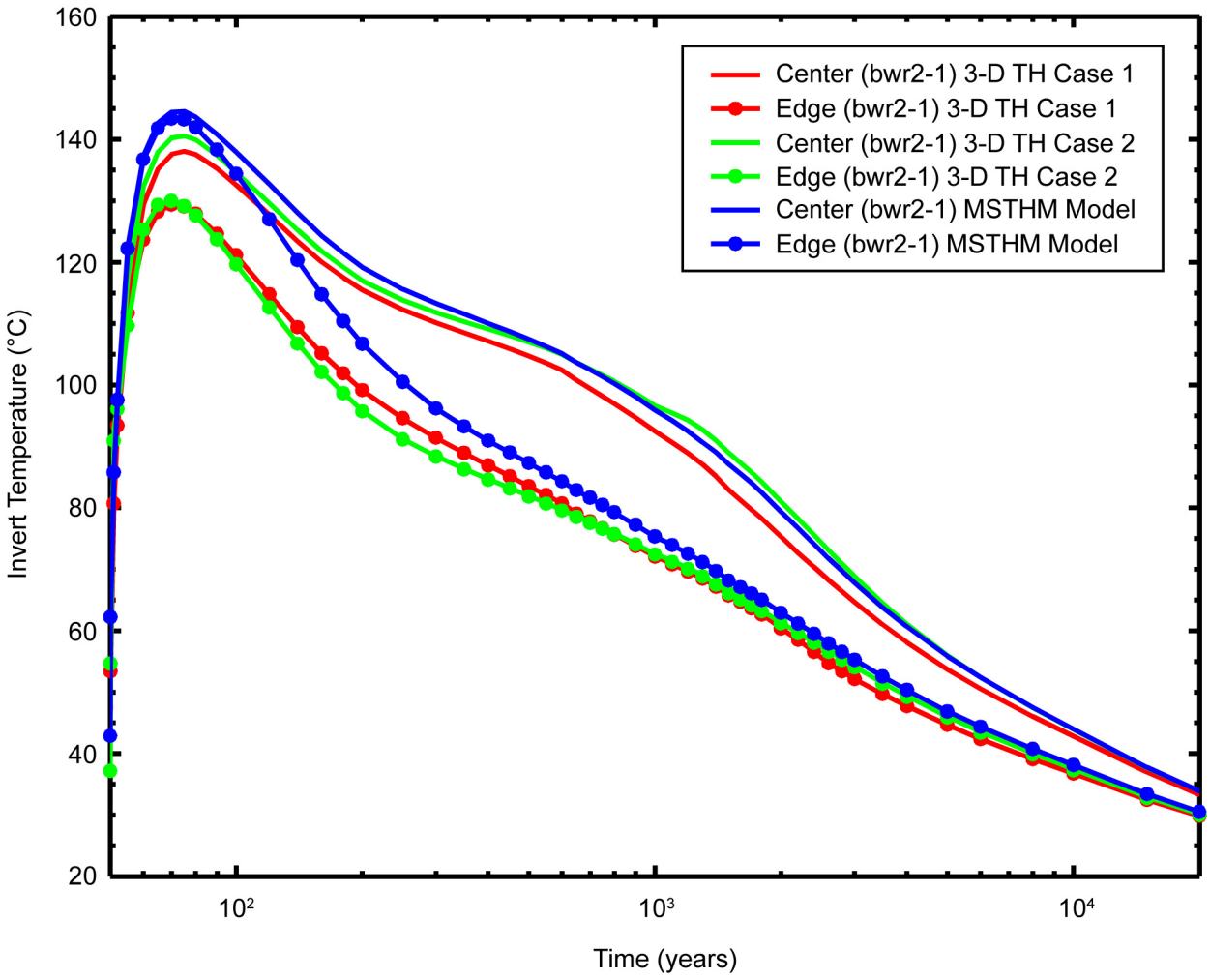

Source: Output DTN: LL0705PA032MST.028.

NOTE: For the 3-D pillar-scale TH model, Case 1 allows advective and diffusive vapor transport along a drift, while Case 2 does not. These results are for the bwr2-1 waste packages located at the repository center and edge. At the repository edge, the bwr2-1 is the fifth waste package from the edge.

Figure 7.8-14[b]. Invert Temperature Predicted by the MSTHM and 3-D Pillar-Scale TH Model Compared at the Repository Center and Edge for the bwr2-1 Waste Package

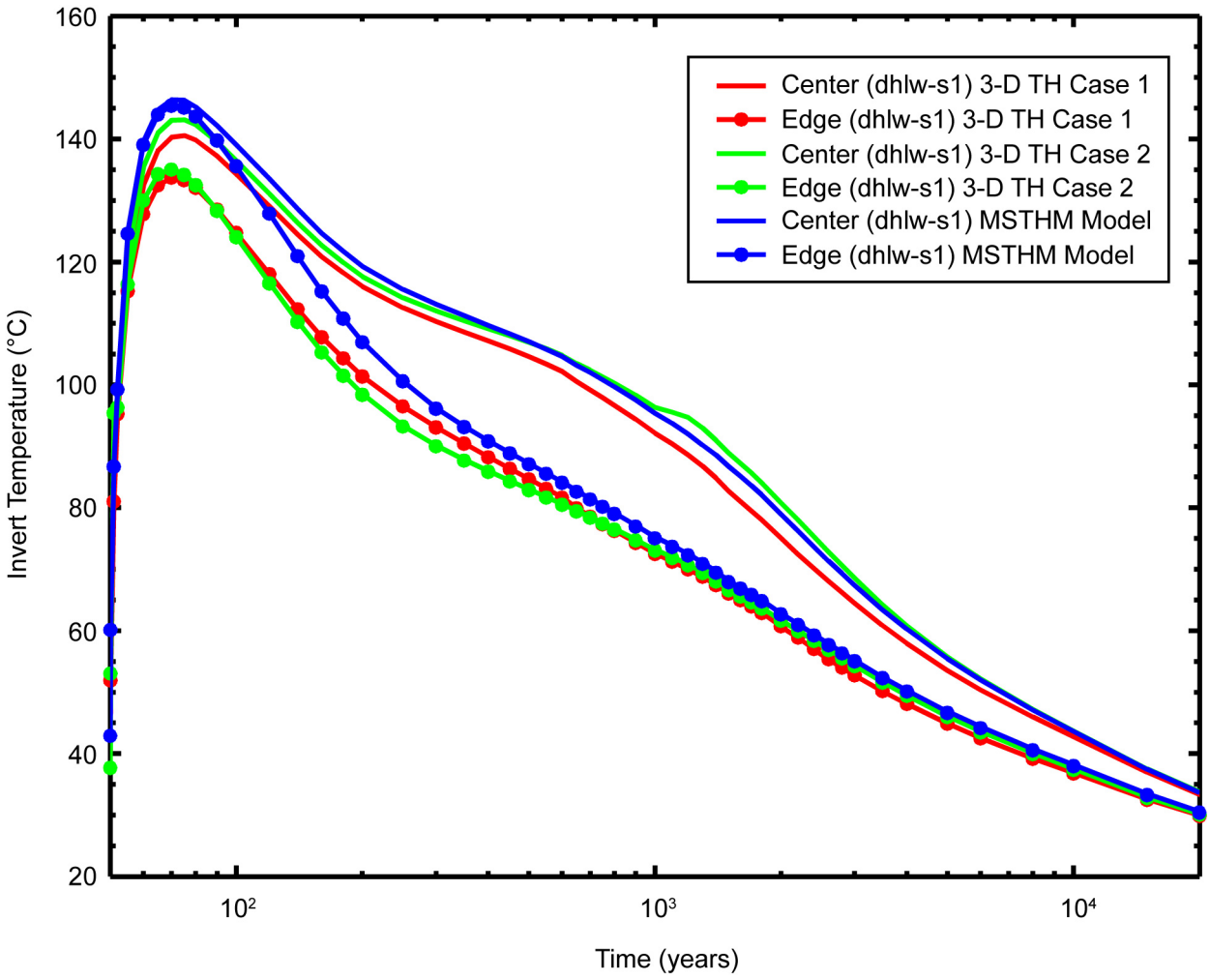

Source: Output DTN: LL0705PA032MST.028.

NOTE: For the 3-D pillar-scale TH model, Case 1 allows advective and diffusive vapor transport along a drift, while Case 2 does not. These results are for the dhlw-s1 waste packages located at the repository center and edge. At the repository edge, the dhlw-s1 is the sixth waste package from the edge.

Figure 7.8-15[b]. Invert Temperature Predicted by the MSTHM and 3-D Pillar-Scale TH Model Compared at the Repository Center and Edge for the dhlw-s1 Waste Package

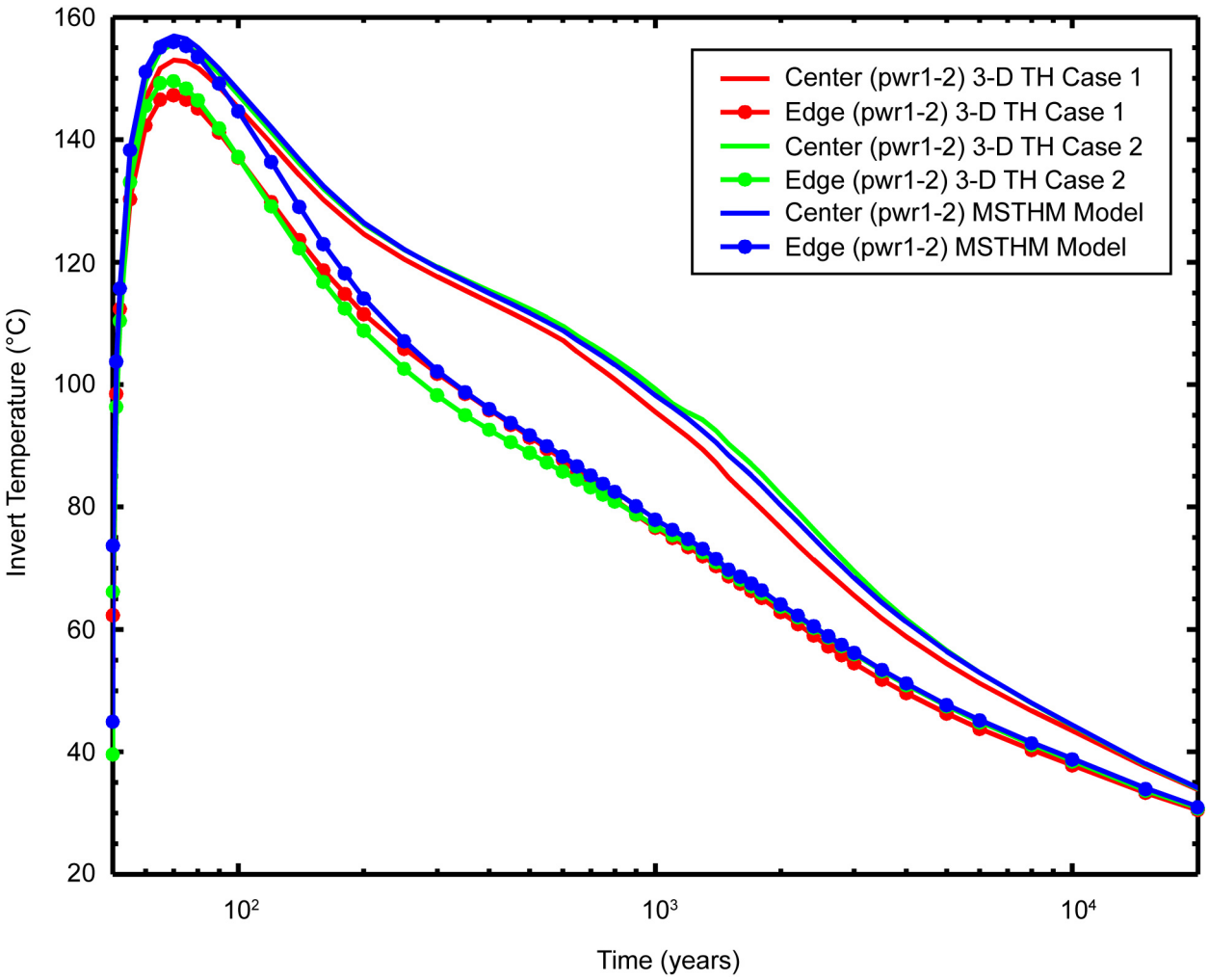

Source: Output DTN: LL0705PA032MST.028.

NOTE: For the 3-D pillar-scale TH model, Case 1 allows advective and diffusive vapor transport along a drift, while Case 2 does not. These results are for the pwr1-2 waste packages located at the repository center and edge. At the repository edge, the pwr1-2 is the seventh waste package from the edge.

Figure 7.8-16[b]. Invert Temperature Predicted by the MSTHM and 3-D Pillar-Scale TH Model Compared at the Repository Center and Edge for the pwr1-2 Waste Package

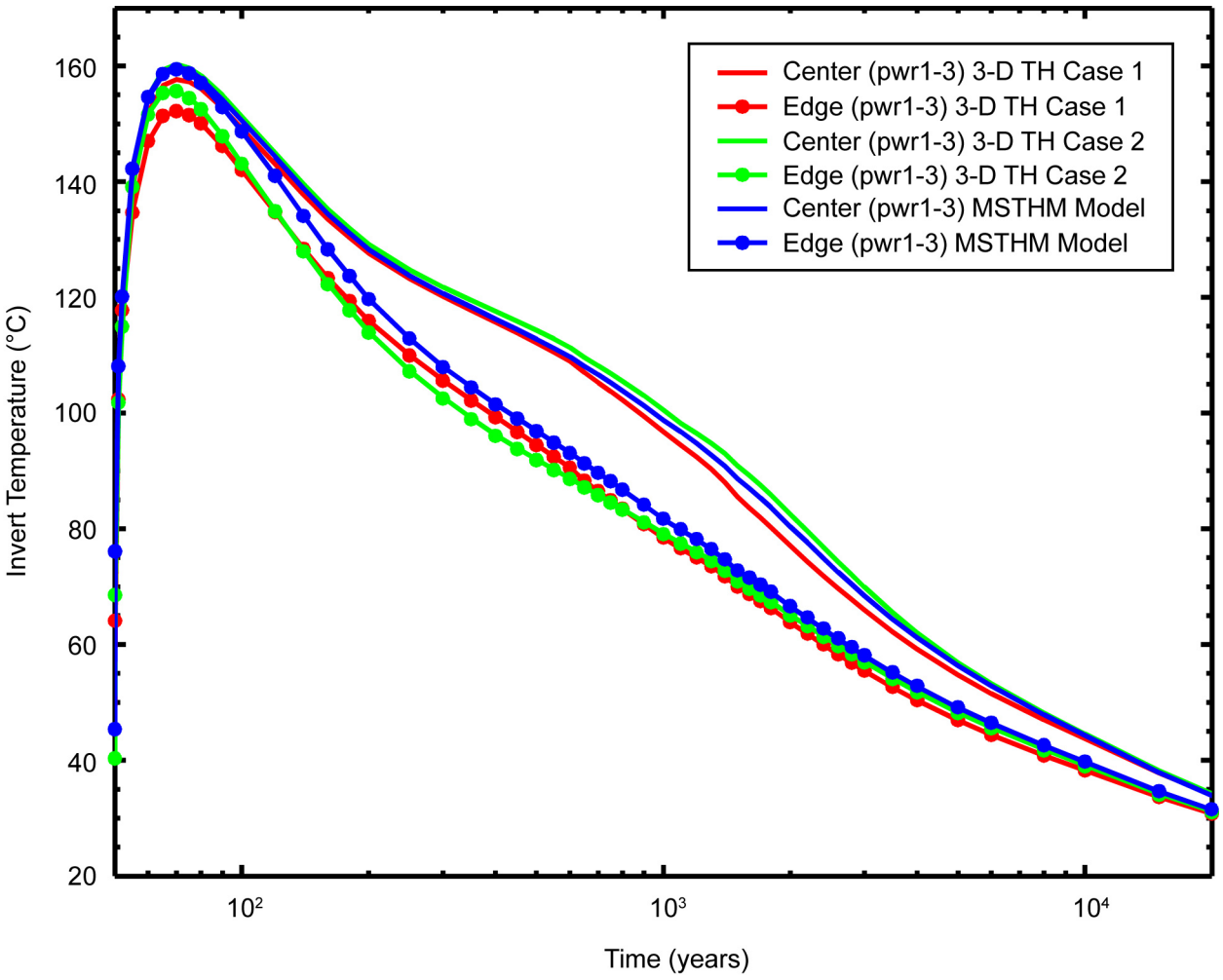

Source: Output DTN: LL0705PA032MST.028.

NOTE: For the 3-D pillar-scale TH model, Case 1 allows advective and diffusive vapor transport along a drift, while Case 2 does not. These results are for the pwr1-3 waste packages located at the repository center and edge. At the repository edge, the pwr1-3 is the eighth waste package from the edge.

Figure 7.8-17[b]. Invert Temperature Predicted by the MSTHM and 3-D Pillar-Scale TH Model Compared at the Repository Center and Edge for the pwr1-3 Waste Package

7.9[b] UPDATED VALIDATION SUMMARY

[The following text is added to the end of Section 7.9[a] of the parent report to expand the validation summary to include the new information added to Section 7.8[a] and Appendix X[a].]

Unsaturated hydrologic properties for the crushed tuff invert ballast are estimated in Appendix X[a] of the parent report. Sensitivity analyses presented in Section 6.3.11 of the parent report show that output from the MSTHM is insensitive to the unsaturated hydrologic properties used for the intragranular porosity of the invert. The intragranular invert liquid-phase saturation varies, but the invert temperature does not (Figure 6.3-63 of the parent report), nor does the invert liquid-phase saturation perturb other MSTHM outputs (e.g., drift wall temperature or *RH*; Figure 6.3-64 of the parent report). This is reasonable because the unsaturated invert cannot store enough moisture to significantly perturb the hydrologic regime within the drift or in the repository near field, and because the intergranular porosity has ample excess intergranular permeability to drain any liquid flux that may occur there.

The invert liquid-phase saturation tracks the *RH* in the environment, shown by the similarity of invert liquid-phase saturation and drift wall liquid-phase saturation in Figures 7.8-2[a] through 7.8-9[a] of the parent report. Relative humidity conditions in the invert, and thus liquid-phase saturation conditions, closely correspond with conditions in the host rock, where there are far greater amounts of water present. Additional analysis presented in Section 6.3.14[a] of the parent report shows that the MSTHM is insensitive to the residual saturation parameter for the intergranular porosity of the invert ballast. This is expected because although the residual saturation affects how much moisture can be stored, the amount stored for repository conditions is not sufficient to perturb other MSTHM outputs. Uncertainty in the invert liquid-phase saturation affects the volumetric moisture content, but substantial uncertainty in this parameter is already accommodated in the approach used for TSPA (SNL 2007 [DIRS 177407], Section 6.3.4.1.1).

Agreement in the invert ballast intragranular liquid-phase saturation predicted by the MSTHM and by the 3-D TH pillar-scale model is discussed in Section 7.8[a] of the parent report and in Section 7.8[b] of this addendum (see Figures 7.8-2[a] through 7.8-9[a] in the parent report). This result confirms that the representation of invert liquid-phase saturation based on the MSTHM, is consistent with the extended domain and dimensionality of the 3-D TH model. In accordance with the foregoing discussion, the representation of invert liquid-phase saturation in the MSTHM is valid for its intended use to represent environmental conditions for diffusive transport of radionuclides in the invert (SNL 2007 [DIRS 177407], Section 6.5.2.3) and invert chemical conditions that affect radionuclide solubility and colloid stability (SNL 2007 [177412], Section 6.15.2; see Appendix XV of the parent report).

Thermal conductivity for the crushed tuff invert ballast material (0.2 W/m-K) is estimated in Appendix IV of the parent report (Table IV-9), based on the simple average (rounded) of a set of laboratory data. This estimate was corroborated independently using the method of Kunii and Smith (1960 [DIRS 153166]; see Appendix XI in the parent report) yielding a closely comparable value of 0.21 W/m-K (Section X.3[a] in the parent report and Appendix X[b] of this addendum). The difference is well within the estimated uncertainty on the estimate (30%; see

Appendix X[b]). This analysis also showed that heat transfer by radiative coupling in the pore space of the invert ballast is not significant (Section X.3[a] of the parent report).

Sensitivity analyses discussed in Section 6.3.2 of the parent report show that output from the MSTHM is insensitive to thermal conductivity of the invert. This result is corroborated by the sensitivity analysis of invert height (Section 6.3.19[a] of the parent report), in which the invert thickness was increased from 0.806 m to 1.32 m, thereby increasing the thermal resistance (thickness divided by conductivity) by more than 50%. This produced changes in temperature and *RH* results output from the MSTHM (Figures 6.3-94[a] through 6.3-97[a] in the parent report) that are small compared to the major sources of uncertainty (host-rock thermal conductivity and percolation flux; estimated for the three-drift validation test case in Section 7.5.3 and Figures 7.5-9 through 7.5-11 of the parent report).

Finally, agreement in the average invert temperature predicted by the MSTHM and by the 3-D TH pillar-scale model is discussed in Section 7.8[b] of this addendum (see Figures 7.8-10[b] through 7.8-17[b]). This result confirms that the representation of invert temperature based on the MSTHM, is consistent with the extended domain and dimensionality of the 3-D TH model. In accordance with the foregoing discussion, the representation of invert temperature in the MSTHM is valid for its intended use to represent environmental conditions for diffusive transport of radionuclides in the invert (SNL 2007 [DIRS 177407], Section 6.5.2.3) and invert chemical conditions that affect radionuclide solubility and colloid stability (SNL 2007 [DIRS 177412], Section 6.15.2; see Appendix XV of the parent report).

8[b]. CONCLUSIONS

[The following correction is made to the DIRS number at the end of the paragraph following item (3) in Section 8.4.3[a] of the parent report.]

8.4.3[b] Acceptance Criterion 3 – Data Uncertainty Is Characterized and Propagated through the Model Abstraction

Other examples are the percolation flux, thermal loading, and host-rock thermal conductivity parameter sets used in the MSTHM, which are also used by the near-field chemistry model for representing seepage composition (SNL 2007 [DIRS 177412]).

[The following new section is added after Section 8.5.8[a] of the parent report.]

8.5.9[b] CR-5154 – Invert Ballast Properties Inconsistent in SAR Design vs. Postclosure Analysis

The condition identified by CR-5154 (now completed in the Corrective Action Program) is addressed by the analysis documented in Addendum 01 of the parent report (Appendix X[a]). CR-5154 referred to the medium for which hydrologic properties of the invert ballast were estimated. In Appendix X[a], the characteristics of a representative graded, compacted material (LTBM-2) are used to estimate hydrologic properties that are used in the multiscale model calculations described in Addendum 01. The LTBM-2 material description is traceable to current engineering information for the invert ballast (BSC 2004 [DIRS 168138]), so the inconsistency identified in CR-5154 is resolved. Whereas the records for CR-5154 show that the

properties analysis was documented in a technical product that has since been cancelled, the estimation of these properties is now documented by Appendix X[a].

9[b]. INPUTS AND REFERENCES

9.1[b] DOCUMENTS CITED

[No modification is required to the existing references for the parent report. The following new references are added to support this addendum.]

168138 BSC (Bechtel SAIC Company) 2004. *Estimation of Mechanical Properties of Crushed Tuff for Use as Ballast Material in Emplacement Drifts.* 800-CYC-SSE0-00100-000-00A. Las Vegas, Nevada: Bechtel SAIC Company. ACC: ENG.20040309.0023; ENG.20050817.0009; ENG.20050829.0017.

178297 BSC 2006. *Technical Work Plan for: Additional Multiscale Thermohydrologic Modeling.* TWP-MGR-PA-000036 REV 02. Las Vegas, Nevada: Bechtel SAIC Company. ACC: DOC.20060825.0001.

113426 Crane, R.A.; Vachon, R.I.; and Khader, M.S. 1977. "Thermal Conductivity of Granular Materials - A Review." Proceedings of the Seventh Symposium on Thermophysical Properties, held at National Bureau of Standards, Gaithersburg, Maryland, May 10-12, 1977. Cezairliyan, A., ed. Pages 109-123. New York, New York: American Society of Mechanical Engineers. TIC: 246057.

108184 Incropera, F.P. and DeWitt, D.P. 1996. *Fundamentals of Heat and Mass Transfer.* 4th Edition. New York, New York: John Wiley & Sons. TIC: 243950.

134666 Keenan, J.H.; Keyes, F.G.; Hill, P.G.; and Moore, J.G. 1969. *Steam Tables, Thermodynamic Properties of Water Including Vapor, Liquid, and Solid Phases (English Units).* New York, New York: John Wiley & Sons. TIC: 246766.

153166 Kunii, D. and Smith, J.M. 1960. "Heat Transfer Characteristics of Porous Rocks." *American Institute of Chemical Engineers Journal, 6,* (1), 71-78. New York, New York: American Institute of Chemical Engineers. TIC: 249321.

177407 SNL (Sandia National Laboratories) 2007. *EBS Radionuclide Transport Abstraction.* ANL-WIS-PA-000001 REV 03. Las Vegas, Nevada: Sandia National Laboratories. ACC: DOC.20071004.0001.

177412 SNL 2007. *Engineered Barrier System: Physical and Chemical Environment.* ANL-EBS-MD-000033 REV 06. Las Vegas, Nevada: Sandia National Laboratories. ACC: DOC.20070907.0003.

181383 SNL 2007. *Multiscale Thermohydrologic Model.* ANL-EBS-MD-000049 REV 03 ADD 01. Las Vegas, Nevada: Sandia National Laboratories. ACC: DOC.20070831.0003.

179354 SNL 2007. *Total System Performance Assessment Data Input Package for Requirements Analysis for Engineered Barrier System In-Drift Configuration*. TDR-TDIP-ES-000010 REV 00. Las Vegas, Nevada: Sandia National Laboratories. ACC: DOC.20070921.0008.

179466 SNL 2007. *Total System Performance Assessment Data Input Package for Requirements Analysis for Subsurface Facilities.* TDR-TDIP-PA-000001 REV 00. Las Vegas, Nevada: Sandia National Laboratories. ACC: DOC.20070921.0007.

9.2[b] CODES, STANDARDS, REGULATIONS, AND PROCEDURES

[The following is the new revision of the procedure used for this addendum.]

SCI-PRO-006, Rev. 07, ICN 0. *Models*. Washington, D.C.: U.S. Department of Energy, Office of Civilian Radioactive Waste Management. ACC: DOC.20080118.0004.

9.3[b] SOURCE DATA, LISTED BY DATA TRACKING NUMBER

[No modification to parent report.]

9.4[b] OUTPUT AND DEVELOPED DATA, LISTED BY DATA TRACKING NUMBER

[The following output DTN listings are added to support this addendum.]

LL0702PA015MST.070. Output for ANL-EBS-MD-000049 Multiscale Thermohydrologic Model for the Mean Host-Rock Thermal Conductivity, 10-Percentile Percolation Flux Case. Submittal date: 02/22/2007.

LL0702PA017MST.072. Output for ANL-EBS-MD-000049 Multiscale Thermohydrologic Model for the Mean Host-Rock Thermal Conductivity, 30-Percentile Percolation Flux Case. Submittal date: 02/14/2007.

LL0702PA019MST.074. Output for ANL-EBS-MD-000049 Multiscale Thermohydrologic Model for the Mean Host-Rock Thermal Conductivity, 50-Percentile Percolation Flux Case. Submittal date: 02/14/2007.

LL0702PA021MST.076. Output for ANL-EBS-MD-000049 Multiscale Thermohydrologic Model for the Mean Host-Rock Thermal Conductivity, 90-Percentile Percolation Flux Case. Submittal date: 02/14/2007.

LL0702PA023MST.078. Output for ANL-EBS-MD-000049 Multiscale Thermohydrologic Model for the Low Host-Rock Thermal Conductivity, 10-Percentile Percolation Flux Case. Submittal date: 02/14/2007.

LL0702PA025MST.080. Output for ANL-EBS-MD-000049 Multiscale Thermohydrologic Model for the High Host-Rock Thermal Conductivity, 90-Percentile Percolation Flux Case. Submittal date: 02/14/2007.

LL0702PA029MST.084. Output for ANL-EBS-MD-000049 Multiscale Thermohydrologic Model for the Low Host-Rock Thermal Conductivity, 10-Percentile Percolation Flux Case. Submittal date: 02/15/2007.

LL0705PA032MST.028. Model-Confidence Building and Sensitivity Studies for ANL-EBS-MD-000049 Multiscale Thermohydrologic Model (MSTHM). Submittal date: 08/23/2007.

[The following DTN listings replace the corresponding listings in Section 9.4[a] of the parent report. The DTN titles were in error and have been corrected as follows:]

LL0703PA011MST.006. Output for ANL-EBS-MD-000049 Multiscale Thermohydrologic Model for the Mean Host-Rock Thermal Conductivity, 10-Percentile Percolation Flux Case. Submittal date: 03/07/2007.

LL0703PA012MST.007. Output for ANL-EBS-MD-000049 Multiscale Thermohydrologic Model for the Mean Host-Rock Thermal Conductivity, 30-Percentile Percolation Flux Case. Submittal date: 03/13/2007.

LL0703PA013MST.008. Output for ANL-EBS-MD-000049 Multiscale Thermohydrologic Model for the Mean Host-Rock Thermal Conductivity, 50-Percentile Percolation Flux Case. Submittal date: 03/13/2007.

LL0703PA014MST.009. Output for ANL-EBS-MD-000049 Multiscale Thermohydrologic Model for the Mean Host-Rock Thermal Conductivity, 90-Percentile Percolation Flux Case. Submittal date: 03/13/2007.

LL0703PA015MST.010. Output for ANL-EBS-MD-000049 Multiscale Thermohydrologic Model for the Low Host-Rock Thermal Conductivity, 10-Percentile Percolation Flux Case. Submittal date: 03/13/2007.

LL0703PA016MST.011. Output for ANL-EBS-MD-000049 Multiscale Thermohydrologic Model for the High Host-Rock Thermal Conductivity, 90-Percentile Percolation Flux Case. Submittal date: 03/13/2007.

LL0703PA017MST.012. Output for ANL-EBS-MD-000049 Multiscale Thermohydrologic Model for the High Host-Rock Thermal Conductivity, 10-Percentile Percolation Flux Case. Submittal date: 03/13/2007.

LL0703PA034MST.016. Output for ANL-EBS-MD-000049 Multiscale Thermohydrologic Model for the Low Host-Rock Thermal Conductivity, 30-Percentile Percolation Flux (P30L) Case. Submittal date: 03/22/2007.

[The following new output data were generated for this addendum.]

MO0712THMHYDDP.000. Thermal-hydrologic Data and Plots. Submittal date: 12/19/2007.

INTENTIONALLY LEFT BLANK

APPENDIX X[b]

HYDROLOGIC PROPERTIES FOR THE INTERGRANULAR POROSITY OF THE INVERT

X.2[b] POROSITY AND RESIDUAL SATURATION FOR THE INTERGRANULAR POROSITY

[The following correction has been made to page X-5[a] of the parent report in the paragraph after Equation X-21[a]. The paragraph contained a reference to the incorrect equation, which has been changed from 6.5.3.3-11 to 6.5.2.3-11.]

Note that this equation agrees with Equation X-12[a] when the pore space is fully saturated with water ($\theta_m = \phi_m$ and $\theta_I = \phi_I$). This equation is also in agreement with Equation 6.5.2.3-11 of *EBS Radionuclide Transport Abstraction* (SNL 2007 [DIRS 177407]).

X.3[b] THERMAL CONDUCTIVITY

[The following new text is added to the end of Section X.3[a] of the parent report, to provide additional confidence in the invert thermal conductivity value used in the MSTHM.]

The value for invert thermal conductivity used in the MSTHM is 0.2 W/m-K, which is obtained from the average of 11 test data, rounding off the result (Table IV-9 of the parent report). The crushed tuff material measured in the laboratory (4-10 sand; Table IV-9 of the parent report) is different from the description of invert ballast (LTBM-2 ballast; Section X.1[a] of the parent report). Additional confidence was then obtained by corroborating the original value (0.2 W/m-K) using an alternative analysis in Appendix X[a] of the parent report, based on the method of Kunii and Smith (1960 [DIRS 153166]; see Appendix XI of the parent report). This method is independent of the test data, based only on the thermal conductivity of the particles and an approximate description of the particle size distribution. The result (0.21 W/m-K) compares closely with the value used in the MSTHM. The uncertainty associated with estimates of this type is ±30% (Crane et al. 1977 [DIRS 113426]), so the difference (0.21 minus 0.20 W/m-K) is well within the uncertainty of the estimate. (A summary of invert thermal conductivity information is included in Section 7.9[b] of this addendum.)

INTENTIONALLY LEFT BLANK